Modeling and mechanism of reactive orange 16 dye adsorption by chitosan-glyoxal/TiO$_2$ nanocomposite: application of response surface methodology

Ahmed Saud Abdulhameed[a], AbdulKarim-Talaq Mohammad[a], Ali H. Jawad[b],*

[a]*Chemistry Department, College of Science, University of Anbar, Ramadi, Iraq,*
email: ahmedchem339@gmail.com (A.S. Abdulhameed), drmohamadtalaq@gmail.com (A.-T. Mohammad)
[b]*Faculty of Applied Sciences, Universiti Teknologi MARA, 40450 Shah Alam, Selangor, Malaysia, Tel. + 60355211721,*
email: ali288@salam.uitm.edu.my, ahjm72@gmail.com (A.H. Jawad)

ABSTRACT

Hybrid cross-linked chitosan-glyoxal/TiO$_2$ nanocomposite (Chi-Gly/TNC) was prepared and employed for the adsorption of reactive orange 16 dye (RO16) from aqueous solution. Response surface methodology (RSM) with 4-level Box–Behnken design (BBD) was applied to optimize RO16 removal efficiency. Various process parameters, viz., loading of TiO$_2$ nanoparticles into Chi-Gly polymeric matrix (A: 0–50%), adsorbent dose (B: 0.04–0.14 g/50 mL), solution pH (C: 4–10), and temperature (D: 30–50°C) were selected for optimization process. Analysis of variance (ANOVA) was incorporated to judge the adequacy of model. The significant simultaneous interactions between input variables on RO16 removal efficiency were clearly observed by interactions between AB, AD, BC, and BD. Applying the method of the desirability function, optimization of TiO$_2$ loading (50% TiO$_2$: 50% chitosan labeled as Chi-Gly/TNC-50), adsorbent dose (0.09 g/50 mL), solution pH ~ 4.0, and temperature at 40°C gave a maximum of 93.2% RO16 removal efficiency by Chi-Gly/TNC-50. The adsorption of RO16 from aqueous solution at optimum input variables by using Chi-Gly/TNC-50 in batch mode was evaluated. The kinetic results were well described by the pseudo-first order kinetic, and the equilibrium data were in agreement with Langmuir and Freundlich isotherm models with maximum adsorption capacity of 390.5 mg/g. The adsorption mechanism was attributed to the dipole-dipole hydrogen bonding interactions, Yoshida H-bonding, n-π stacking interactions, and electrostatic attractions.

Keywords: Cross linking; Chitosan; Glyoxal; Nanocomposite; Titanium dioxide; Reactive orange 16

1. Introduction

A variety of dyes are produced by different industries like textile, paper, plastic, leather, cosmetics and pharmaceuticals [1]. Most of these dyes are discharged into wastewater that affect human's health and ecological environment [2,3]. Reactive orange 16 (RO16) as an anionic dyes, belongs to the azo dyes and soluble in aqueous media [4]. The presence of azo (N=N) group in RO16 structure causes low biodegradability and makes a risk of environmental system [5]. However, most of dyes that discharged to the wastewater were azo dyes [6]. Thus, from the environmental viewpoint,

removing azo dye from waste waters is an important step before releasing it into the aquatic environment. Recently, there are many technologies are available for removing various dyes from aqueous solution such as flocculation [7], adsorption [8], photo catalysis [9], and oxidation process [10]. Adsorption technique has the superiority on others technologies for the removal of dyes from wastewater due to its high efficient and low working cost, in addition to reduce formation harmful substances [11–13].

Chitosan is an abundant biopolymer derivative from chitin by deacetylation process [14]. Chitosan has amino (–NH$_2$) and hydroxyl (–OH) functional groups that active adsorption sites for removal of dyes [15], and metal ions [16]. Application of unmodified chitosan as an adsorbent has many disadvantages because of its low surface area,

*Corresponding author.

dissolution in acidic solutions, low mechanical properties and high swelling index [17]. Thus, chemical modification of chitosan by using cross-linking is an important step to reduce hydrophobicity, increase the stability of chitosan in acidic solutions, and enhance the mechanical properties [18]. The incorporation of inorganic nanomaterials such as nano scale titanium dioxide (TiO_2) into polymeric matrix of chitosan will be responsible for improving its adsorption capacity, compatibility, mechanical properties, and chemical stability [19].

Recently, chitosan and TiO_2 complement each other to produce chitosan-TiO_2 composite materials which exhibited multi-functional performance for many potential applications such as wastewater treatment [20], photo catalysis [21], antibacterial activity [22], drug delivery [23], and biosensor [24]. In spite many desirable properties of TiO_2 nanoparticles such as high surface area, high chemical stability, insolubility in water, relatively low cost, and nontoxicity [25]. However, TiO_2 nanoparticles alone are not a successful material in water treatment technology because of the difficulty of separation and nanoparticles recovery from aqueous solution by conventional filtration and/or centrifugation processes. Among various response surface designs available in response surface methodology (RSM), Box-Behnken Design (BBD) is more labor efficient, and quite suitable for fitting second order polynomial equations with the number of experimental factors equal or greater than three [26].

Therefore, the objective of the current work is to investigate the feasibility of using hybrid cross linked chitosan-glyoxal/TiO_2 nanocomposite (Chi-Gly/TNC) to be potential biosorbent for the removal of RO16 dye from aqueous solution, and to optimize the input variables for maximum removal efficiency by using BBD. The applied input variables were loading of TiO_2 nanoparticles into chitosan matrix, adsorbent dose, solution pH, and temperature. RO16 as tri-aromatic acid dye molecules was chosen as a model pollutant due to its complicated molecular structure and non-biodegradability.

2. Martials and methods

2.1. Chemical and reagents

Chitosan flakes (degree of deacetylation $\geq$ 75), titanium (IV) dioxide P-25 and glyoxal solution were supplied from Sigma–Aldrich. Reactive Orange (RO16) was purchased from ACROS, Organics (chemical formula: $C_{20}H_{17}N_3Na_2O_{11}S_3$, MW: 617.54, λ_{max} = 495 nm). Fig. 1 shows molecular structure of RO16. Acetic acid (CH_3COOH), sodium hydroxide (NaOH) and hydrochloric acid (HCl) were obtained from R&M Chemicals. All chemicals and reagents used in this work were analytical grade with high purity. Ultra-pure water (18.2 MΩ /cm) was utilized in this study.

2.2. Preparation of chitosan-glyoxal/TiO₂ nanocomposites

Chitosan-glyoxal/TiO_2 nanocomposite was synthesized according to the method described by Mohammad et al., [27]. 1 g of chitosan flakes were dissolved in 50 mL of 5% acetic acid solution, and then the solution was left with stirrer for 24 h. The viscous solution was injected into of 1000 mL NaOH (0.5 M) solution by using 10 mL syringe
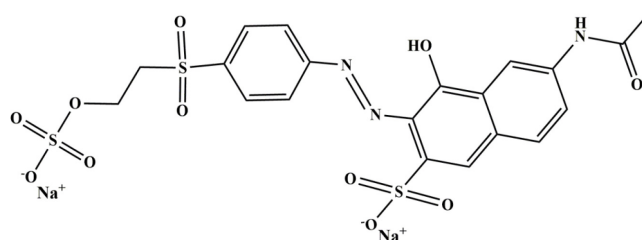

Fig. 1. Molecular structure of RO16.

with rate 1 mL/min to prepare chitosan beads that washed with distilled water to remove the trace of NaOH solution. The crosslinking reaction was carried out by adding 90 mL of 1% glyoxal solution to the chitosan beads with gentle stirring under heating in water bath at temperature 40°C for 2 h to prepare the chitosan-glyoxal beads (Chi-Gly). After that, Chi-Gly beads were extensively washed with distilled water and air dried for 24 h. Then, the Chi-Gly beads were pounded and dried in the oven. After that, The Chi-Gly beads were sieved to a constant particle size of 150 < particle size > 250 µm for further applications. To fulfill the requirement of the optimization process that pre-determined by BBD, a series of chitosan-glyoxal/TiO_2 nanocomposites (Chi-Gly/TNC) were synthesized by loading different ratios of TiO_2 nanoparticles with chitosan flakes before dissolving by 5% acetic acid solution, as described above and following the preparation procedure. The chitosan-glyoxal/TiO_2 nanocomposite with fixed mixing ration of (25% TiO_2 nano particles: 75% chitosan flakes). While, the chitosan-glyoxal/TiO_2 nanocomposite with fixed mixing ration of (50% TiO_2 nano particles: 50% chitosan flakes) is labeled as Chi-Gly/TNC-50 throughout this work. The chitosan-glyoxal/TiO_2 nanocomposite powder was sieved to constant particle size of 150 < particle size > 250 µm for further applications. The scheme of crosslinked chitosan-glyoxal/TiO_2 nanocomposite preparation is shown in Fig. 2.

2.3. Characterization of Chi-Gly/TNC-50

The surface morphology of Chi-Gly/TNC-50 before and after RO16 adsorption was examined *via* scanning electron microscope with energy dispersive X-ray analyzer (SEM-EDX, Zeiss Supra 40 VP, Germany). The samples were coated with gold by a Polaron SC 515 sputter coater prior to analysis to make the samples electrically conductive. The functional groups of samples were identified by Fourier transform infrared (FTIR) Spectroscopy (Perkin-Elmer, Spectrum RX I). The samples were milled with potassium bromide, KBr (spectrophotometric grade). This powder was compressed into a thin pellet. The thin pellet was placed in the cell holder and inserted into FTIR spectrophotometer to be analyzed. All the spectra were recorded within the wave numbers range of 4000–450 cm^{-1}.

2.4. Design of experiments

The current work is focused on four-level Box–Behnken design (BBD) in response surface methodology (RSM) to optimize the loading of TiO_2 nanoparticles into chitosan-gly-
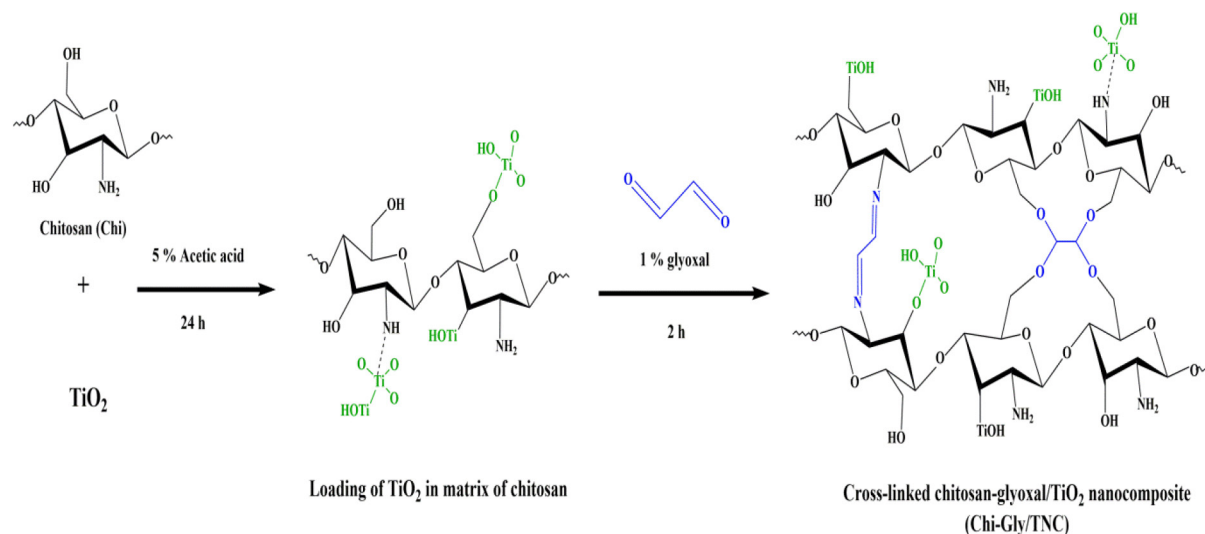
Fig. 2. Scheme of preparation cross linked chitosan-glyoxal/TiO$_2$nanocomposite.

oxal (Chi-Gly) polymeric matrix, adsorbent dose, solution pH, and temperature. The significant of each single factor, interactions and quadratic terms in the optimization process was determined by using statistical analysis computer software [Design expert software version 11.0 Stat ease, Minneapolis, USA]. Each factor was varied at three different levels −1, 0 and +1 signifying low, medium and high values. The arrangement of the factorial design is shown in Table 1.

A total of 29 experiments were employed in this work to evaluate the effects of the four input variables on RO16 removal efficiency. Anon-linear regression method was used to fit the second order polynomial [Eq. (1)] to the experimental data and to identify the relevant model terms. Considering all the linear terms, square terms and linear by linear interaction items, the quadratic response model can be described as:

$$Y = \beta_0 + \sum \beta_i X_i + \sum \beta_{ii} X_i^2 + \sum \sum \beta_{ij} X_i X_j \tag{1}$$

where Y is an objective to optimize the response, β_0 is the constant coefficient, β_i is the linear coefficient, β_{ii} is the quadratic coefficient and β_{ij} is the interaction coefficient, while X_i and X_j are the coded values of the independent factors.

The design consisted of 29 runs was carried out to optimize the levels of the selected input variables, *viz.*, A: TiO$_2$ loading (A: 0–50%) (zero value means no TiO$_2$ loaded into Chi-Gly, while 50% means that 50% of TiO$_2$ nanoparticles were loaded to 50% chitosan in the polymeric matrix of Chi-Gly in order to produce Chi-Gly/

TNC-50), B: adsorbent dose (B: 0.04–0.14 g) in 50 mL of 50 mg/L RO16 solution, C: pH (C: 4–10) and D: temperature (D: 30–50°C). A certain amount of adsorbent was added to 125 mL Erlenmeyer flasks containing 50 mL of 50 mg/L RO16 solution. The flasks were capped and agitated in an isothermal water bath shaker (Memmert, water bath, Model WNB7-45, Germany) at a fixed shaking speed of 100 strokes/min at fixed shaking time of 60 min. The range of the variables was chosen based on preliminary experiments. After shaking process, the adsorbent were separated by syringe filter (0.45 µm) and the changes in RO16 concentrations were determined using a HACH DR 2800 Direct Reading Spectrophotometer at maximum wave length of 493 nm. The dye (RO16) removal, DR (%) of was determined using Eq. (2).

$$DR\ \% = \frac{(C_o - C_e)}{C_o} \times 100 \tag{2}$$

where C_o (mg/L) and C_e (mg/L) are the initial and equilibrium concentrations of RO16 dye in aqueous solution, respectively. The actual BBD experimental design matrix is given in Table 2.

2.5. Batch adsorption study

It was proven from run 18 (experiment 18) in Table 2 that the maximum removal efficiency of RO16 from aqueous solution can be achieved at the following experi-

Table 1
Coded and actual variables and their levels

Coded variables	Actual variables	Level 1 (–1)	Level 2 (0)	Level 3 (+1)
A	TiO$_2$ loading (%)	0	25	50
B	Adsorbent dose (g)	0.04	0.09	0.14
C	pH	4	7	10
D	Temperature (°C)	30	40	50

Table 2
The 4-factors BBD matrix and experimental data for RO16 removal efficiency

Run	A: TiO$_2$ loading (%)	B: Adsorbent dose (g)	C: pH	D: T (°C)	Dye removal (%)
1	0	0.04	7	40	10.9
2	50	0.04	7	40	36.9
3	0	0.14	7	40	25.7
4	50	0.14	7	40	83.4
5	25	0.09	4	30	66
6	25	0.09	10	30	15
7	25	0.09	4	50	84
8	25	0.09	10	50	18
9	0	0.09	7	30	14.5
10	50	0.09	7	30	40.4
11	0	0.09	7	50	25
12	50	0.09	7	50	81.2
13	25	0.04	4	40	53.6
14	25	0.14	4	40	92.7
15	25	0.04	10	40	13
16	25	0.14	10	40	25
17	0	0.09	4	40	68.7
18	50	0.09	4	40	93.2
19	0	0.09	10	40	13
20	50	0.09	10	40	28
21	25	0.04	7	30	19.9
22	25	0.14	7	30	37.4
23	25	0.04	7	50	18
24	25	0.14	7	50	71.3
25	25	0.09	7	40	36.1
26	25	0.09	7	40	35.5
27	25	0.09	7	40	36.8
28	25	0.09	7	40	34.9
29	25	0.09	7	40	35.4

[0 TiO$_2$ loading means Chi-Gly, 25% TiO$_2$ loading means Chi-Gly/TNC-25, and 50% TiO$_2$ loading means Chi-Gly/TNC-50].

mental TiO$_2$ loading (A: 50%, meaning that 50% chitosan: 50% nano TiO$_2$), adsorbent dose (B) 0.09 g in 50 mL), pH ~ 4 (C), and temperature (D) 40°C. Therefore, these optimum experimental conditions were adopted in the batch adsorption study. The batch adsorption experiments for RO16 adsorption were carried out by following the same above-mentioned procedure with different initial RO16 concentration (20–200 mg/L) and contact time. The adsorption capacity of RO16 at equilibrium was determined using Eq. (3).

$$q_e = \frac{(C_o - C_e)V}{W} \qquad (3)$$

where C_o (mg/L) and C_e (mg/L) are the initial and equilibrium concentrations of RO16 in aqueous solution. V is Volume of the RO16 solution (L) while, W is the weight of Chi-Gly/TNC-50 (g).

3. Results and discussion

3.1 Response surface methodology

3.1.1 Box-Behnken design

Total 29 experiments (runs) were designed by BBD (Table 2). For the four examined factors the TiO$_2$ loading (A), adsorbent dose (B), solution pH (c), and temperature (D) were considered as the independent process factors and their individual and interactive effects on the RO16 removal efficiency (as response) were investigated using the BBD approach. A quadratic polynomial model was chosen for developing the mathematical relationship between the response and the process factors.

The empirical relationships between tested factor and response are presented by Eq. (4):

$$\text{RO16 removal}(\%) = +35.74 + 17.11A + 15.72B - 28.86C \qquad (4)$$
$$+8.68D + 7.95AB + 7.56AD - 6.78BC + 8.95BD + 10.29C^2$$

where A, B, C and D are the coded levels of TiO$_2$ loading, adsorbent dose, pH and temperature, respectively. Based on the coefficients in equation of (4) the TiO$_2$ loading (A), adsorbent dose (B) and temperature (D) shows appositive effect on RO16 removal (%) efficiency, while pH (C) has a negative effect [28]. Hence, it can be inferred that by increasing the TiO$_2$ loading, adsorbent dose and temperature, RO16 removal (%) raises on the other hands, whereas by increasing solution pH, RO16 removal (%) was decreased.

3.1.2 Effect of input variables

The perturbation plot was employed to investigate the effect of four input variables simultaneously on the RO16 removal efficiency as shown in Fig. 3. As can be seen, there are four input variables are the key factors for obtaining maximum RO16 removal efficiency. A sharp curvature for the TiO$_2$ loading (variable A) indicates that the RO16 removal efficiency was so sensitive to this variable. Generally, as adsorbent dose (variable B) increase the RO16 removal efficiency increases as well. A relatively steep curvature in solution pH (variable C) implies that the RO16 removal efficiency was sensitive to this variable. The curve of temperature (variable D) indicates sensitivity of the response in working temperature levels.

3.1.3 Analysis of variance (ANOVA)

The experimental data for removal efficiency were statistically analyzed by ANOVA and the results are presented in Table 3. Results of ANOVA are based on the F-values, sum of the squares and p-values to determine the significant factors. The model F-value of 37.45 for
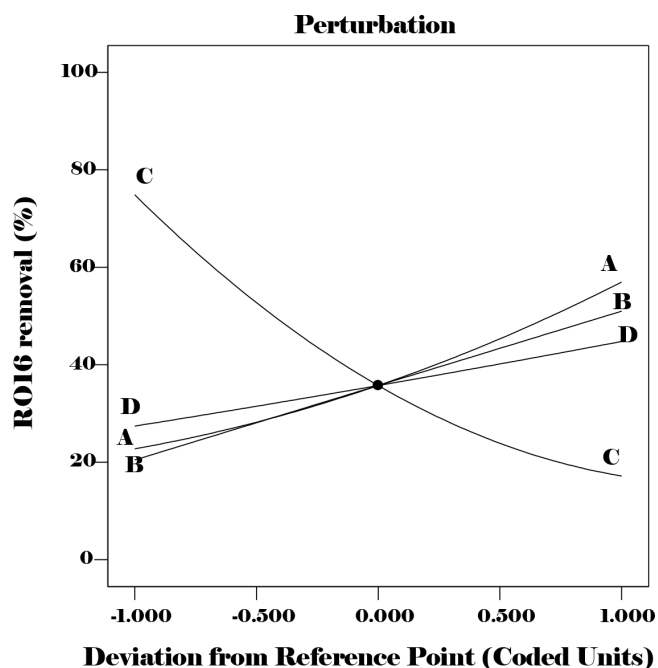
Fig. 3. Perturbation plots for the dye removal efficiency of RO16. (A) TiO$_2$ loading, (B) adsorbent dose, (C) pH, and (D) temperature.

RO16 dye and the corresponding p-value are <0.0001, indicates the model is statistically significant [29]. These further appear that there is only a 0.01% chance for the model F-value that could happen due to noise. The adequate precision tests the signal to noise ratio where a ratio

greater than 4 is valuable [30]. Ratio of the model is 21.2, which indicate an adequate signal. Thus, this model can be applied to navigate of the design space. The model appears coefficient of determination (R^2) value of 0.97 and an adjusted-R^2 value of 0.95 which is high and indicates a high correlation between the actual and the predicted values. Based on Table 3, the values of model terms Prob > F < 0.0500 indicate that factors are significant under selected conditions. The linear terms of A, B, C and D, the quadratic term of C^2, the interaction between AB, AD, BC and BD are significant model terms. However, the model terms with p-value > 0.05 is insignificant, therefore insignificant terms were excluded from the model to enhance fitting of the model.

Graphical method can be utilized to validate model and also characterizes the nature of residuals distribution of the model. Plot of normal probability is generally utilized to test the distribution of the residuals of the model [31,32] as shown in Fig. 4. The normal probability plot of the residuals shows no serious violation from the assumptions underlying of the analyses, where points on this plot lie significantly close to a straight line. The perfect normal distributions of the residuals indicate the accuracy of the assumptions, as well as the independence of the residuals. Fig. 5 demonstrates the relationship between the predicted and actual values of RO16 dye removal (%) by Chi-Gly/TNC-50. The predicted and actual values are close to each other on the straight line, which indicates the statistical validation of the model. This close correlation between the actual and predicted values of percentage dye removal was also exhibited by the values of R^2 (0.97) and adjusted R^2 (0.95) which are observed to be close to one**.**

Table 3
Analysis of variance (ANOVA) of the response surface quadratic model for RO16 removal efficiency

Source	Sum of Squares	Df	Mean Square	F-value	p-value	Remarks
Model	19045.73	14	1360.41	37.45	<0.0001	Significant
A-TiO$_2$ loading	3513.71	1	3513.71	96.73	<0.0001	Significant
B-Adsorbent dose	2797.46	1	2797.46	77.01	<0.0001	Significant
C-pH	9991.33	1	9991.33	275.04	<0.0001	Significant
D-Temp.	904.80	1	904.80	24.91	0.0002	Significant
TiO$_2$ loading × Adsorbent dose	252.65	1	252.65	6.96	0.0195	Significant
TiO$_2$ loading × pH	22.71	1	22.71	0.6250	0.4424	Insignificant
TiO$_2$ loading × Temp.	228.92	1	228.92	6.30	0.0250	Significant
Adsorbent dose × pH	184.01	1	184.01	5.07	0.0410	Significant
Adsorbent dose × Temp.	320.05	1	320.05	8.81	0.0102	Significant
pH × Temp.	56.25	1	56.25	1.55	0.2338	Insignificant
TiO$_2$ loading 2	110.39	1	110.39	3.04	0.1032	Insignificant
Adsorbent dose 2	0.0003	1	0.0003	8.95906	0.9977	Insignificant
pH 2	686.87	1	686.87	18.91	0.0007	Significant
Temp. 2	0.8194	1	0.8194	0.0226	0.8828	Insignificant
Residual	508.57	14	36.33			
Cor Total	19554.30	28				

Normal Plot of Residuals
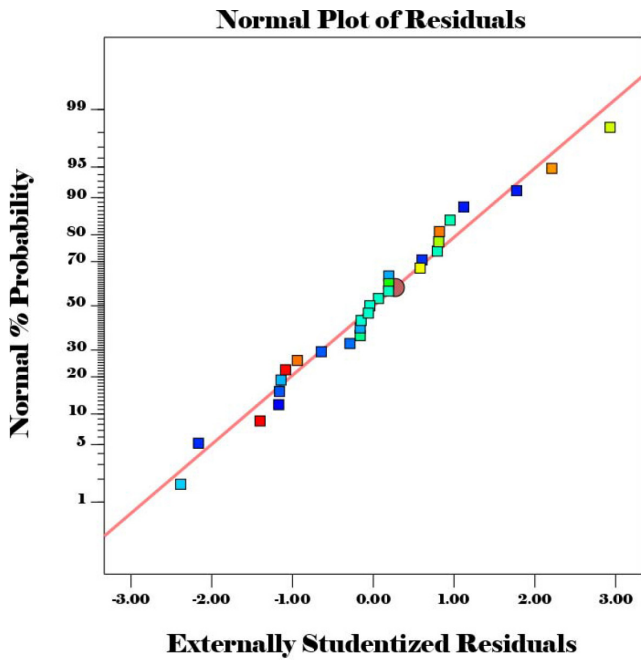
Fig. 4. Normal probability plot of residuals for RO16 removal efficiency.
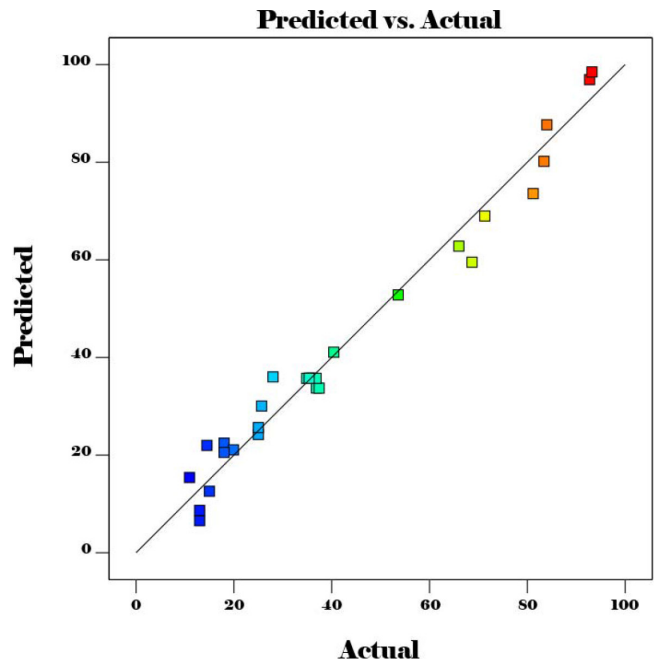
Predicted vs. Actual

Fig. 5. Plot of the relationship between the predicted and actual values of RO16 removal efficiency (%).

3.1.4. Three-dimensional (3D) response surfaces

In order to get distinctive understanding of responsive relationships between independent variables and RO16 removal (%) efficiency (response), three-dimensional (3D) response surfaces for the RO16 removal (%) were determined based on the quadratic model. The significant interaction between each two input variables (as given in Table 3) was investigated. The interaction effect of TiO_2 loading (A) and adsorbent dose (B) was signifi-

cant (p-value = 0.019 as obtained from Table 3) on RO16 removal efficiency. The other two input factors of solution pH ~ 7 and temperature at 40°C were simultaneously kept constant within the experimental range. The 3-D surfaces and 2-D contours plots for AB interaction are presented in Figs. 6a and 6b respectively. Generally, it is found that the RO16 removal efficiency increases by increasing the TiO_2 loading and adsorbent dose. The remarkable improvement in RO16 removal efficiency (from 10.93% to 93.23%) with increasing the loading of
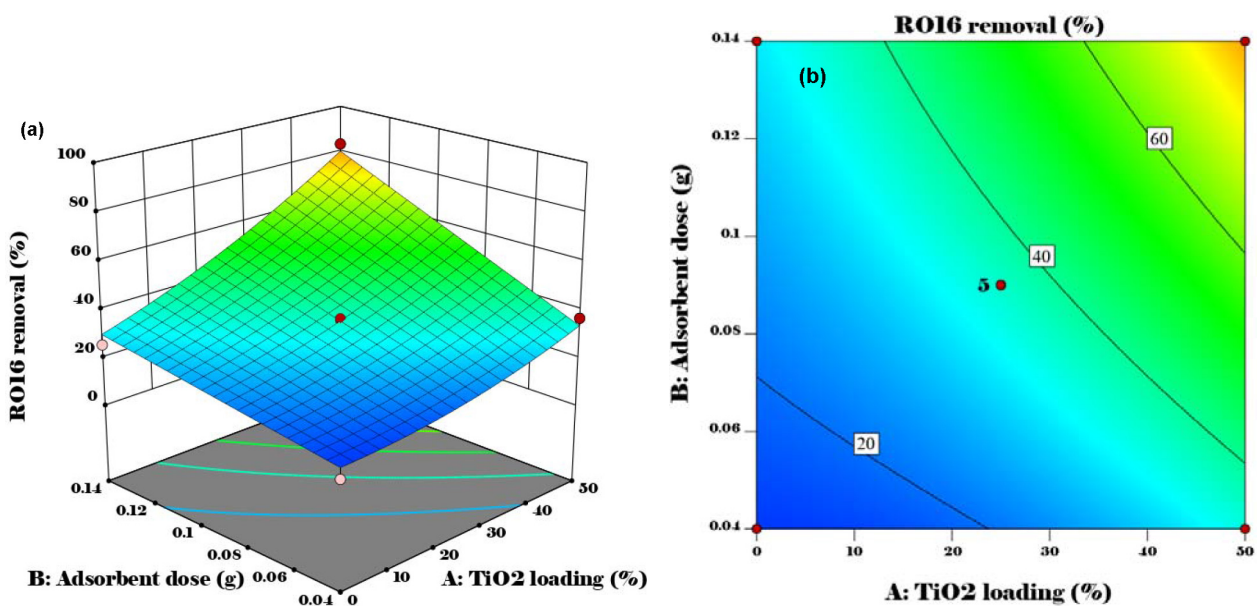

Fig. 6. (a) 3D response surface plot and, (b) contour plot for RO16 removal efficiency showing interaction between TiO_2 loading (A) and adsorbent dose (B).

TiO_2 nanoparticles into cross linked chitosan matrix up to 50% chitosan: 50% nano TiO_2. In fact, loading of TiO_2 nanoparticles into polymeric matrix of Chi-Gly leads to enhance the surface area of Chi-Gly/TNC-50 and introducing new types of hydroxyl groups on the surface Chi-Gly/TNC-50. The terminal hydroxyl and bridging hydroxyl groups on the surface of Chi-Gly/TNC-50 will be protonated and converted to the positive oxonium ions especially in acidic aqueous environment [33]. On the other hand, the sulfonate group ($–SO_3H$) in the molecular structure of the RO16 can be converted in aqueous medium into active negative sulfonate group ($–SO_3^-$). Consequently, a strong electrostatic (columbic) attraction between positively charged oxonium ions on the surface of Chi-Gly/TNC-50 with negatively charged sulfonate groups of RO16 [27]. Regarding adsorbent dose (B), it is found that the RO16 removal efficiency increases from 10.93% to 93.23% by increasing Chi-Gly/TNC-50 dose up to 0.09 g/50 mL, which can be ascribed to the greater availability of the exchangeable adsorption sites [34].

It was also found that the interaction effect of adsorbent dose (B) and solution pH (C) was significant (P = 0.041) on RO16 removal efficiency. The other two input variables of TiO_2 loading and temperature at 40°C were simultaneously kept constant within the experimental range. The 3-D surfaces and 2-D contours plots for BC interaction are presented in Figs. 7a and 7b, respectively. A positive charge of the Chi-Gly/TNC-50 can be obtained at pH ~ 4, preferring the adsorption of negatively charged species such as RO16 anionic species. As a result, a strong electrostatic (columbic) attraction between positively charged protonated amino groups on the Chi-Gly/TNC-50 surface with negatively charged sulfonate group of RO16 can be obtained, thus increases RO16 removal efficiency as describe in Eq. (5).

$$R – NH_3^+ + RO16 – SO_3^- \leftrightarrow R – NH_3^+ – –SO_3^- – RO16 \qquad (5)$$

From Eq. (5) it is observed that the does influences the availability of the exchangeable adsorption sites for adsorption and solution pH is responsible for surface charge of adsorbent, therefore their interaction effect is influential in the response.

The interaction effect of temperature (D) with TiO_2 loading (A) and adsorbent dose (B) were significant on RO16 removal efficiency as shown in the 3-D surfaces and 2-D contours plots of Figs. 8a and 8b and Figs. 9a and 9b, respectively. The other two independent variables of adsorbent dose (0.09 g of Chi-Gly/TNC-50) and pH at ~ 7 were simultaneously kept constant within the experimental range for interaction of temperature (D) and TiO_2 loading (A) (Fig. 6), while for interaction of temperature (D) and adsorbent dose (B) the other two input variables of TiO_2 loading (50% TiO_2: 50% chitosan known as Chi-Gly/TNC-50) and pH at ~7 were simultaneously kept constant within the experimental range (Fig. 7). From Figs. 8 and 9, reactive orange 16 removal efficiency increases with increasing temperature up to 50°C. This can be attributed to the increasing in diffusion process of the RO16 molecules across the internal structure of the adsorbent [35], and also indicates that the adsorption process is an endothermic process in nature [36].

3.1.5. Model validation for RO16

In order to test the accuracy of the optimization process, the model was validated by two groups of different combination of variables (TiO_2 loading, adsorbent dose, pH and temperature) each within their experimental ranges. The model predicted values and actual values were utilized to check the validity of BBD model (Table 4). In accordance with Table 4, the maximum removal (%) obtained from actual values were 96.1 and 94.46, which is in good agreement with the predicted values of the BBD model. This indicates that the BBD model can be successfully applied to optimize the removal efficiency of the RO16 dye using Chi-Gly/TNC-50.
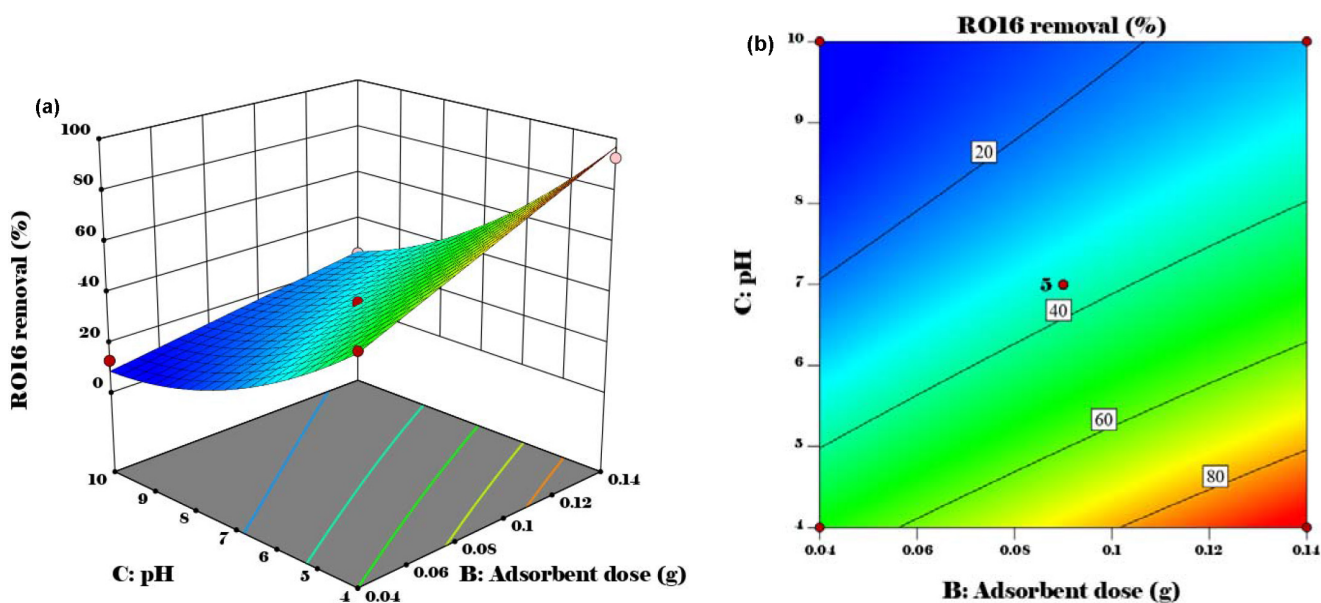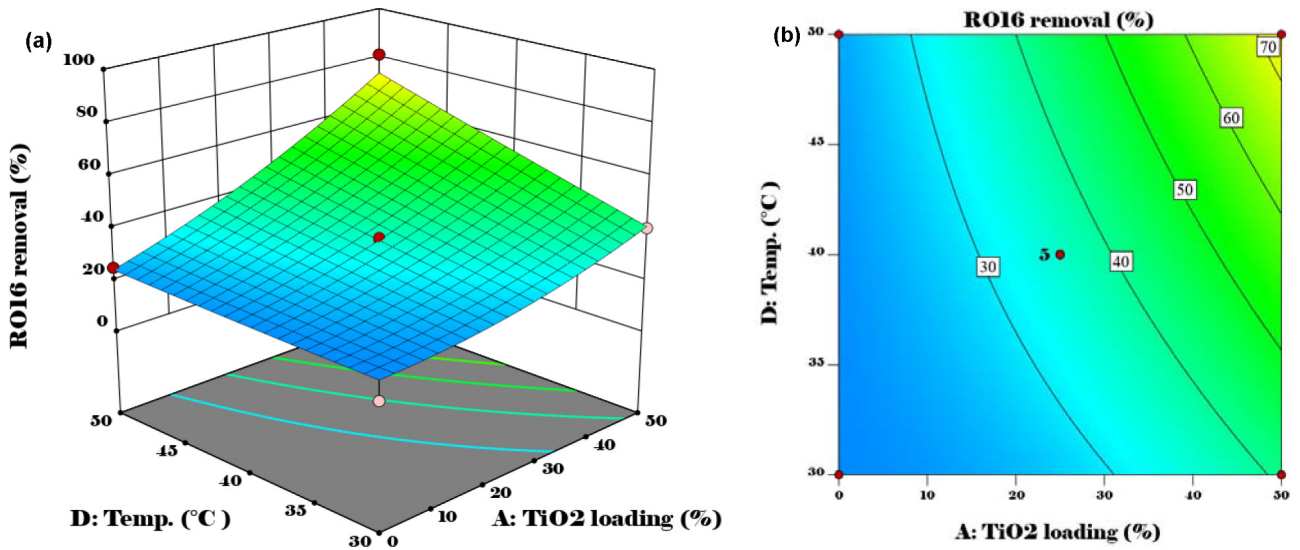

Fig. 7. (a) 3D response surface plot, and (b) contour plot (b) of RO16 removal efficiency showing interaction between adsorbent dose (B) and pH (C).

Fig. 8. (a) 3D response surface plot, and (b) contour plot of RO16 removal efficiency showing interaction between TiO$_2$ loading (A) and temperature (D).
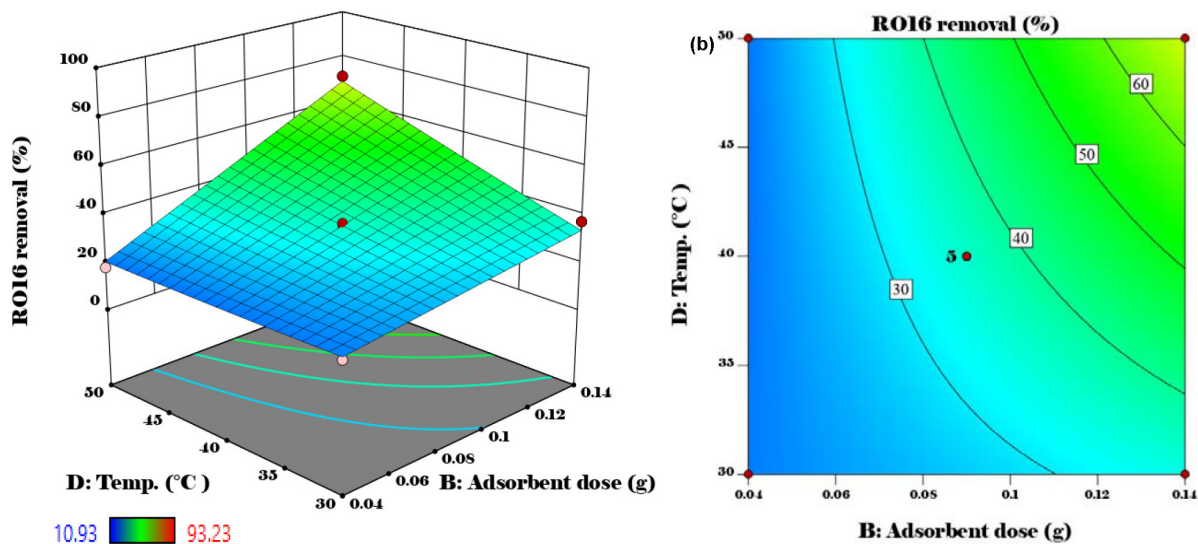

Fig. 9. (a) 3D response surface plot, and (b) contour plot of RO16 removal efficiency showing interaction between adsorbent dose (B) and temperature (D).

3.2 Adsorption study

The adsorption study of RO16 by Chi-Gly/TNC-50 was performed at different initial RO16 concentration (20–200 mg/L) and contact time as shown in Fig. 10, by keeping

Table 4
The model predicted values and actual values of the validity of BBD model

Run	TiO$_2$ loading (%)	Adsorbent dose (g)	pH	Temp. (°C)	RO16 removal (%)	
					Predicted	Actual
1	50	0.11	4.16	37.73	99.24	96.1
2	50	0.13	7.34	49.79	93.45	94.46

other input variables that given in Table 2 (Run or experiment 18) simultaneously constant within this experiment. As depicted in Fig. 10, the experimental data reveal that the adsorption capacity at equilibrium increases from 21.8 to 254.4 mg/g, with increase in the initial RO16 concentration from 20 to 200 mg/L. This was attributed to a greater collision rate between RO16 molecules and Chi-Gly/TNC-50 by increasing the initial RO16 concentration. Furthermore, the time to reach equilibrium also increased with the increase in initial RO16 concentration.

3.3. Kinetic modeling

In order to figure out the adsorption mechanism, the non-linear pseudo-first-order (PFO) model and pseudo-second-order (PSO) models were used to test the experimental
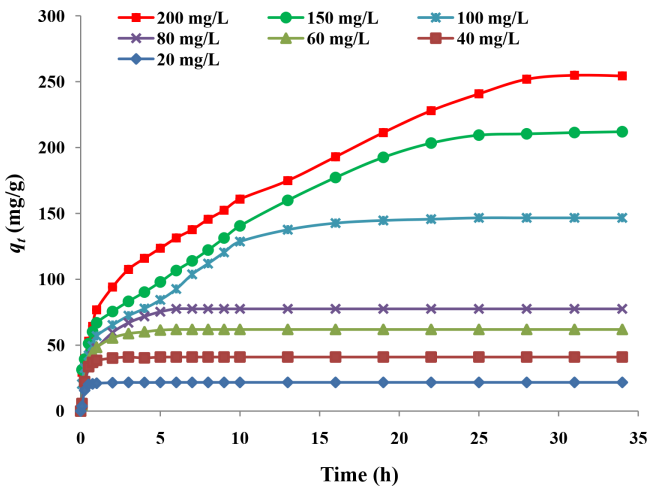
Fig. 10. Effect of contact time and initial concentration on the adsorption of RO16 dye by Chi-Gly/TNC-50 (initial pH of solution = pH 4, adsorbent dose = 0.09 g, temperature = 313 K, agitation speed = 100 strokes and volume of solution = 200 mL).

data of initial concentration. The Lagergren [37] PFO model is expressed by Eq. (6).

$$q_t = q_e \left(1 - \exp^{-k_1 t}\right) \tag{6}$$

The non-linear form of the PSO model [38] is described by Eq. (7).

$$q_t = \frac{q_e^2 k_2 t}{1 + q_e k_2 t} \tag{7}$$

q_e: amounts of RO16 adsorbed by Chi-Gly/TNC-50 at equilibrium (mg/g); q_t: amounts of RO16 adsorbed Chi-Gly/TNC-50 at time t (mg/g); k_1: PFO rate constant (1/h); k_2: PSO rate constant (g/mg h); t: Time (h)

The kinetic data was fit using the nonlinear form of the PFO and PSO models. The kinetic parameters are recorded in Table 5. From Table 5 it was found that the adsorption of RO16 by the Chi-Gly/TNC-50 follows the PFO model in terms of higher correlation coefficient values R^2. Moreover, the q values calculated (q_{cal}) from PFO model were more consistent with the q values experimental (q_{exp}) than those calculated from the PSO. Generally, the k_2 values decrease with the increase in initial dye concentrations from 100 to

400 mg/L. The decreased k_2 values indicates a decrease in the adsorption rate, thereby prolonging the time to attend equilibrium. This result is in a good agreement with adsorption of methyl orange dye (MO) by composite crosslinked chitosan [27].

3.4. Isotherm modeling

The adsorption isotherm is the most meaningful information which describes how the adsorbate molecules distribute between the solid-liquid phases when the adsorption process reaches an equilibrium state. Various isotherm models such as Langmuir, Freundlich, and Temkin were used to explain the equilibrium characteristics of adsorption. The Langmuir isotherm model Langmuir [39] describes the monolayer adsorption process on uniform adsorption sites and is expressed by Eq. (8).

$$q_e = \frac{q_{max} k_a C_e}{1 + k_a C_e} \tag{8}$$

q_e: Adsorbed amount of RO16 at equilibrium (mg/g); C_e: RO16 concentration at equilibrium (mg/L); q_{max}: Langmuir maximum adsorption capacity (mg/g); K_a: Langmuir constant (L/mg).

The equilibrium data were also fitted to the Freundlich isotherm model [40], which is expressed by Eq. (9).

$$q_t = K_f C_e^{1/n} \tag{9}$$

K_f: Freundlich constant ((mg/g) (L/mg)$^{1/n}$)
$1/n$: adsorption intensity of the system.

Temkin isotherm model takes into account the heat of adsorption of all molecules in the layer would decrease linearly rather than logarithmic with coverage [41]. The model is given by Eq. (10).

$$q_t = \frac{RT}{b_T} \ln\left(K_T C_e\right) \tag{10}$$

K_T: Temkin isotherm constant (L/mg); R: universal gas constant [8.314J/(molK)]; T: (K) is the absolute temperature (K); b_T: Heat of adsorption (J/mol).

The nonlinear plots of the tested isotherms models relate to Eqs. (8), (9) and (10) are shown in Fig. 11,

Table 5
PFO and PSO kinetic parameters for RO16 adsorption on Chi-Gly/TNC-50

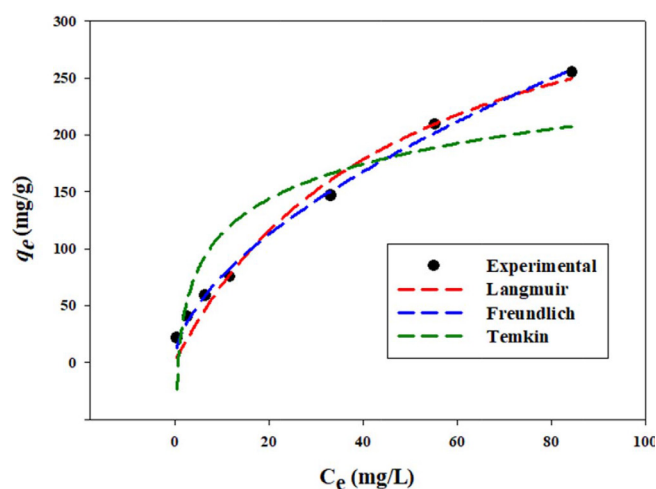| Concentration (mg/L)	q_{eexp} (mg/g)	PFO			PSO		
		q_{ecal} (mg/g)	k_1 (1/h)	R^2	q_{ecal} (mg/g)	$k_2 \times 10^{-4}$ (g/mg h)	R^2
20	21.6	21.8	4.32	0.97	22.4	33.0	0.88
40	40.3	40.9	3.05	0.99	42.3	12.0	0.94
60	58.8	61.4	1.7	0.99	64.3	4.0	0.98
80	75.4	76.8	0.95	0.98	81.9	2.0	0.93
100	146.6	144.1	0.22	0.90	161	0.20	0.93
150	209.4	210.6	0.13	0.89	253.8	0.05	0.91
200	254.9	241.4	0.14	0.89	286.3	0.05	0.92

Fig. 11. Langmuir, Freundlich, and Temkin isotherm plots for the adsorption of RO16 dye on Chi-Gly/TNC-50 at 40°C.

Table 6
Parameters of the Langmuir, Freundlich and Temkin isotherm models for RO16 adsorption on Chi-Gly/TNC-50 at 40°C

Adsorption isotherm	Parameter	Value
Langmuir		
	q_m (mg/g)	390.5
	K_a (L/mg)	0.021
	R^2	0.98
Freundlich		
	K_f (mg/g) (L/mg)$^{1/n}$	20.1
	n	1.7
	R^2	0.99
Temkin		
	K_T (L/mg)	0.24
	b_T (J/mol)	58.6
	R^2	0.82

and other isotherm parameters are recorded in Table 6. According to high R^2 values (Table 6), the adsorption equilibrium follows Langmuir and Freundlich isotherms indicates homogeneous and heterogeneous mode of adsorption [42]. The Chi-Gly/TNC-50 shows good adsorptive property toward RO16 with relatively high adsorption capacity of 390.5 mg/g. The adsorption capacity of RO16 by Chi-Gly/TNC-50 was compared with various adsorbents as given in Table 7. From Table 7, it can be concluded that the Chi-Gly/TNC-50 possesses a relatively high adsorption capacity, suggesting that it may be a promising material for the removal of reactive dyes from aqueous solutions.

3.5. Proposed adsorption mechanism

The proposed adsorption mechanism of RO16 by Chi-Gly/TNC-50 is sketched in Fig. 12. Based on the various functional groups available on the surface of Chi-Gly/TNC-50, the adsorption mechanism of RO16 can be assigned to the various interactions e.g., dipole-dipole hydrogen bonding interactions (Fig. 12a), Yoshida H-bonding (Fig. 12b) and n-π stacking interactions (Fig. 12c). In fact, there are two types of hydrogen bonding can be occurred between Chi-Gly/TNC-50 and molecu-

Table 7
Comparison of the adsorption capacity of reactive orange 16 dye by various adsorbents

| Adsorbents	Dose	pH	T (°C)	q_{max} (mg/g)	Ref.
Chitosan-glyoxal/TiO$_2$ nanocomposite	0.09 g/100 mL	4	40	390.5	This study
Coagulation/activated carbon	0.25 g/L	–	25	509	[43]
Chitosan-epichlorohydrine film	2.50 mg·cm^{-2}/250 mL	4	25	356.50	[44]
Residual brewery yeast	0.7 g/200 mL	3	35	340	[45]
Polyaniline/bacterial extracellular	0.15 g/100 mL	3	50	293.2	[46]
Chitosan /Poly Itaconic Acid	0.015 g/50 mL	4	37	288	[47]
Brazilian-pine fruit activated carbon	0.05 g/50 mL	2–3	25	239	[48]
Cross-linked chitosan/sepiolite composite	0.2 g/100 mL	3	30	190.96	[49]
Paper sludge activated carbon	0.1 g/100 mL	2	30	178	[50]
Ananas Comosus leaves activated carbon	0.1 g/100 mL	2-3	30	147.05	[51]
Chitosan- EGDE biofilm	1 mg·cm^{-2}/250 mL	4	30	131.2	[8]
Sewage sludge	0.4 g/40 mL	2	25	114.7	[52]
Carbonized fish scale	1 g/L	7	50	105.8	[53]
Aqai palm stalk	2.5 g/20 mL	2	25	62.9	[54]
Ethylenediamine modified rice hull	0.06 g/100 mL	4	25	60.24	[55]
Humin immobilized on silica	0.2 g/10 mL	1	25	19.45	[56]
Surfactant zeolites	10 g/10 mL	10	25	12.6	[57]
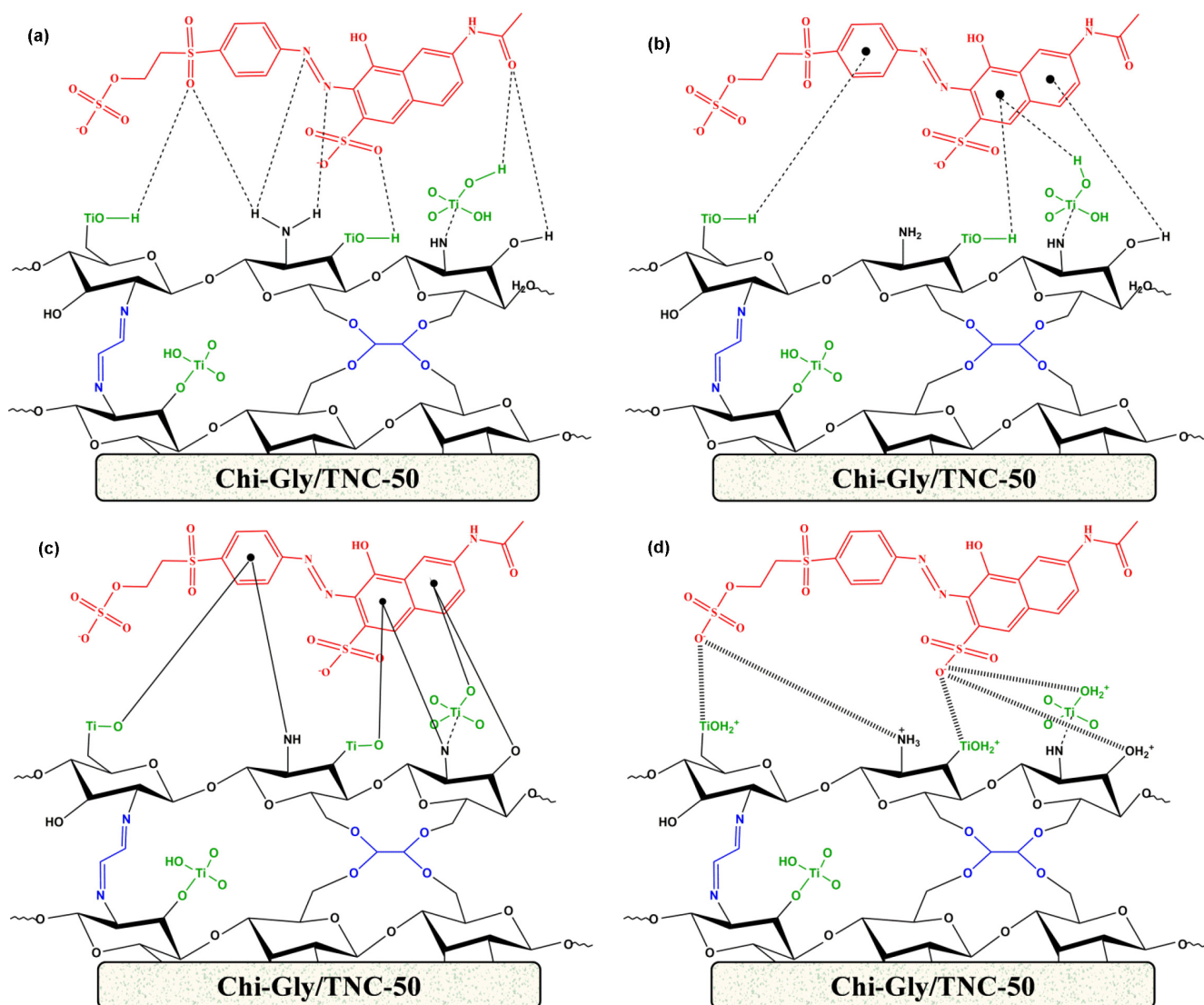
Fig. 12. Illustration of the possible interaction between Chi-Gly/TNC-50 and RO16: (a) dipole-dipole hydrogen bonding interactions, (b) Yoshida H-bonding, (c) n-π stacking interactions, and (d) electrostatic attraction.

lar structure of RO16, the common type is dipole-dipole hydrogen bonding interactions that occurs between available hydrogen in the surface of Chi-Gly/TNC-50 with oxygen and nitrogen atoms available in the molecular structure of RO16 as shown in Fig. 12a, while the second type is Yoshida H-bonding that occurs between –OH in the surface of Chi-Gly/TNC-50 with aromatic ring of dye [58], as shown in Fig. 12b. Another possible interaction is n-π interaction which is generally occurred where the lone pair electrons on an oxygen atom are delocalized into the π orbital of an aromatic ring of dye [59], as shown in Fig. 12c. Electrostatic attractions between negatively charged sulfonate (SO$_3^-$) acid groups of RO16 and the positively charged functional groups available on the surface of Chi-Gly/TNC-50 as shown in Fig. 12d. Similar adsorption mechanism was proposed for adsorption of reactive red 120 and methyl orange by a biofilm of cross-linked chitosan- ethylene glycol diglycidyl ether [8].

3.6. Characterization

3.6.1. SEM-EDX analysis

The surface morphology of the Chi-Gly/TNC-50 before and after R016 adsorption was investigated by SEM-EDX analysis. The SEM images at magnification power 3000× a company with EXD analysis are presented in Figs. 13a and 13b for Chi-Gly/TNC-50 before and after RO16 adsorption, respectively. Fig. 13a shows the surface morphology of Chi-Gly/TNC-50 was unsmooth and heterogeneous in nature with various visible cavities distributed randomly. The representative EDX analysis indicates that the main elements presented in the polymeric matrix of Chi-Gly/TNC-50 were carbon, titanium and oxygen. On the other hand, the surface of Chi-Gly/TNC-50 after RO16 adsorption (Fig. 13b) was changed to be more compact with less visible cavities on the outer surface, which can be attributed to the RO16 molecules loaded on the adsorbent surface. As for representative EDX
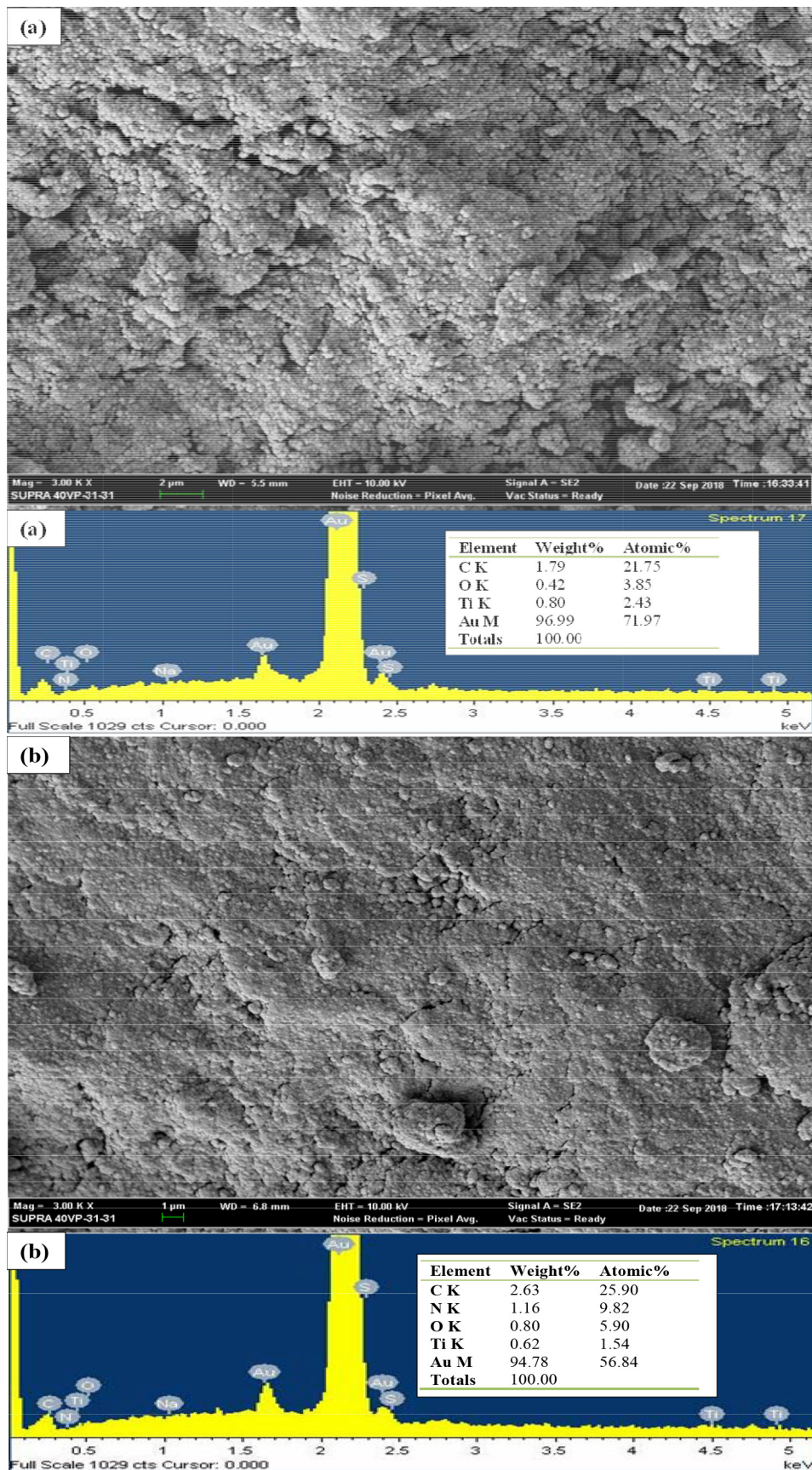
Fig. 13. SEM images and EDX spectra for (a) Chi-Gly/TNC-50 before adsorption, and (b) Chi-Gly/TNC-50 after RO16 adsorption.

analysis, it was also observed that the Chi-Gly/TNC-50 consist mainly of C, N, O, and Ti. The slight increment in the C and O content of Chi-Gly/TNC-50 after RO16 adsorption (Fig. 13b) can be attributed to the RO16 loaded on the surface of Chi-Gly/TNC-50. The appearances of the Au peaks in all spectra are attributed coating process with gold in order to improve electric conduction and enhance the images quality.

3.6.2. FTIR analysis

FTIR spectroscopy was used to identify the functional groups that are responsible for adsorption of RO16 from aqueous solution. FTIR spectrum of crosslinked chitosan-glyoxal/TiO$_2$ nanocomposite –50 was obtained in the range of 450–4000 cm^{-1}, and it is shown in Fig. 14a. Various peaks can be observed in FTIR spectrum of Chi-Gly/TNC-50. The peak at ~3500 cm^{-1} can be ascribed to intermolecular hydrogen bonds and the overlap between O-H and N-H stretching vibration, while characteristic peak at ~2900 cm^{-1} was attributed to the C-H stretching of –CH and –CH$_2$ groups [60]. The peak appearing at 1150 cm^{-1} corresponded to the stretching vibration of C-O in chitosan molecule on C-3 and C-6 position, while peaks at ~1320 cm^{-1} and ~1260 cm^{-1} can be attributed to C-N amide I stretching vibration and amide II stretching vibration, respectively [61]. The peak at ~1650 cm^{-1} is attributed to the imine bond (C=N) result from the Schiff-base reaction between carbonyl groups of glyoxal and amino groups of chitosan [62]. The band located at 770 cm^{-1} is attributed to the Ti-O-Ti stretching while bands at 2851 and 3429 cm^{-1} are attributed to surface hydroxyl groups O-H of TiO$_2$ [22,27]. These bands indicate incorporation of nano-TiO$_2$ into polymeric matrix of Chi-Gly. Finally, the FTIR of Chi-Gly/TNC-50 after RO16 adsorption is presented in Fig. 14b. After RO16 adsorption (Fig. 14b), a new band appears at~1500 cm^{-1} (C=C stretch in aromatic ring) can be assigned to the poly aromatic ring of RO16 dye loaded on Chi-Gly/TNC-50 surface. Moreover, a clear reduction of some bands can be observed of the C=N band and obvious

shift can be observed of the amide II stretching vibration, which may reconfirm the involvement of the Chi-Gly/TNC-50 functional groups with RO16 molecules.

4. Conclusion

In the lab scale study, 4-level Box–Behnken design (BBD) in response surface methodology (RSM) was used to optimize the loading of TiO$_2$ nanoparticles into chitosan-glyoxal (Chi-Gly) polymeric matrix to be a potential biosorbent for reactive orange (RO16) from aqueous solution. Various input variables, viz., loading of TiO$_2$ nanoparticles into Chi-Gly matrix (A: 0-50%), adsorbent dosage (B: 0.04–0.14 g/50 mL), solution pH (C: 4–10), and temperature (D: 30–50°C) were optimized by using BBD for efficient removal for RO16. The highest RO16 removal efficiency was observed by simultaneous interactions between AB, AD, BC and BD. The optimum TiO$_2$ loading, adsorbent dosage, solution pH, and temperature were (50% TiO$_2$: 50% chitosan), 0.09 g/50 mL, 4.0, and 40°C. The adsorption of RO16 from aqueous solution under optimum operation conditions was investigated. The adsorption kinetic results were well described by the pseudo-first order kinetic, and the equilibrium data were best fitted to Langmuir and Freundlich isotherm models with maximum adsorption capacity of 390.5 mg/g. The adsorption mechanism included mainly dipole-dipole hydrogen bonding interactions, Yoshida H-bonding, n-π stacking interactions, and electrostatic attractions.

Fig. 14. FTIR spectra for (a) Chi-Gly/TNC-50 before adsorption and (b) Chi-Gly/TNC-50 after adsorption RO16 dye.

References

[1] O. León, A. Muñoz-Bonilla, D. Soto, D. Pérez, M. Rangel, M. Colina, M. Fernández-García, Removal of anionic and cationic dyes with bioadsorbent oxidized chitosans, Carbohydr. Polym., 194 (2018) 375–383.

[2] H.N. Bhatti, A. Jabeen, M. Iqbal, S. Noreen, Z. Naseem, Adsorptive behavior of rice bran-based composites for malachite green dye: isotherm, kinetic and thermodynamic studies, J. Mol. Liq., 237 (2017) 322–333.

[3] A. Kanwal, H.N. Bhatti, M. Iqbal, S. Noreen, Basic dye adsorption onto clay/MnFe$_2$O$_4$ composite: a mechanistic study, Water Environ. Res., 89 (2017) 301–311.

[4] M.C. Nayak, A.M. Isloor, A. Moslehyani, N. Ismail, A.F. Ismail, Fabrication of novel PPSU/ZSM-5 ultra filtration hollow fiber membranes for separation of proteins and hazardous reactive dyes, J. Taiwan Inst. Chem. Eng., 82 (2018) 342–350.

[5] V. Kecić, Đ. Kerkez, M. Prica, O. Lužanin, M. Bečelić-Tomin, D.T. Pilipović, B. Dalmacija, Optimization of azo printing dye removal with oak leaves-nZVI/H$_2$O$_2$ system using statistically designed experiment, J. Clean. Prod., 202 (2018) 65–80.

[6] N.C. Fernandes, L.B. Brito, G.G. Costa, S.F. Taveira, M.S.S. Cunha–Filho, G.A.R. Oliveira, R.N. Marreto, Removal of azo dye using Fenton and Fenton-like processes: Evaluation of process factors by Box–Behnken design and ecotoxicity tests, Chem.-Biol. Interact., 291 (2018) 47–54.
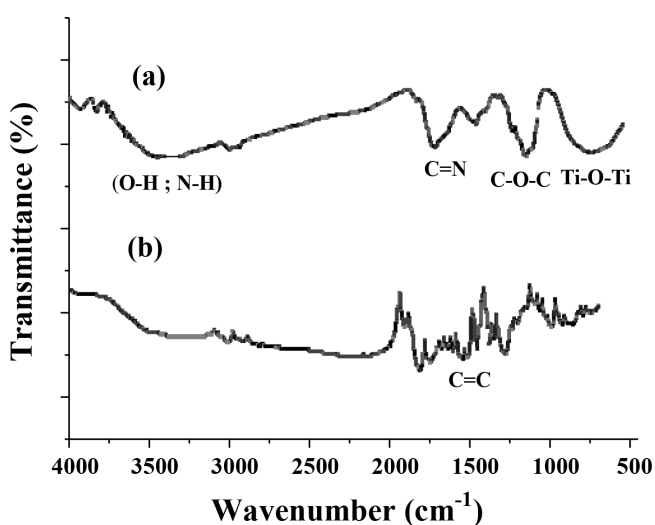
[7] J. Dotto, M.R. Fagundes-Klen, M.T. Veit, S.M. Palácio, R. Bergamasco, Performance of different coagulants in the coagulation/flocculation process of textile wastewater, J. Clean. Prod., 208 (2019) 656–665.

[8] A.H. Jawad, N.F.H. Mamat, B.H. Hameed, K. Ismail, Biofilm of cross-linked Chitosan-Ethylene Glycol Diglycidyl Ether for removal of Reactive Red 120 and Methyl Orange: Adsorption and mechanism studies, J. Environ. Chem. Eng., 7(2) (2019) 102965.

[9] M.A. Nawi, S. Sabar, A.H. Jawad, W.W. Ngah, Adsorption of Reactive Red 4 by immobilized chitosan on glass plates: Towards the design of immobilized TiO_2–chitosan synergistic photo catalyst-adsorption bilayer system, Biochem. Eng. J., 49 (2010) 317–325.

[10] Z. Eskandari, A. Talaiekhozani, M.R. Talaie, F. Banisharif, Enhancing ferrate (VI) oxidation process to remove blue 203 from wastewater utilizing MgO nanoparticles, J. Environ. Manage., 231 (2019) 297–302.

[11] G. Sharma, M. Naushad, A. Kumar, S. Rana, S. Sharma, A. Bhatnagar, M.R. Khan, Efficient removal of coomassie brilliant blue R-250 dye using starch/poly (alginic acid-cl-acrylamide) nanohydro gel, Process Saf. Environ. Prot., 109 (2017) 301–310.

[12] M. Naushad, Z.A. ALOthman, M.R. Awual, S.M. Alfadul, T. Ahamad, Adsorption of rose Bengal dye from aqueous solution by amberlite Ira-938 resin: kinetics, isotherms, and thermodynamic studies, Desal. Water Treat., 57 (2016) 13527–13533.

[13] A.B. Albadarin, M.N. Collins, M. Naushad, S. Shirazian, G. Walker, C. Mangwandi, Activated lignin-chitosan extruded blends for efficient adsorption of methylene blue, Chem. Eng. J., 307 (2017) 264–272.

[14] A.H. Jawad, M.A. Nawi, H.M. Mohamed, L.D. Wilson, Oxidation of chitosan in solution by photo catalysis and product characterization, J. Polym. Environ., 25(3) (2017) 828–835.

[15] C. Li, T. Lou, X. Yan, Y.Z. Long, G. Cui, X. Wang, Fabrication of pure chitosan nanofibrous membranes as effective absorbent for dye removal, Int. J. Biol. Macromol., 106 (2018) 768–774.

[16] L. Zhang, Y. Zeng, Z. Cheng, Removal of heavy metal ions using chitosan and modified chitosan, A review, J. Mol. Liq., 214 (2016) 175–191.

[17] M.A. Nawi, A.H. Jawad, S. Sabar, W.W. Ngah, Photo catalytic-oxidation of solid state chitosan by immobilized bilayer assembly of TiO_2–chitosan under a compact household fluorescent lamp irradiation, Carbohydr. Polym., 83 (2011) 1146–1152.

[18] A.H. Jawad, M.A. Nawi, Characterizations of the photo catalytically-oxidized cross-linked chitosan-glutaraldehyde and its application as a sub-layer in the TiO_2/CS-GLA bilayer photo catalyst system, J. Polym. Environ., 20(3) (2012) 817–829.

[19] A.C.M. Oliveira, M.S. Santos, L.M. Brandão, R.N. Yerga, J.L.G. Fierro, M.S. Leite, R.T. Figueiredo, Chitosan-modified TiO_2 as photo catalyst for ethanol reforming under visible light, Chem. Pap., 71 (2017) 1129–1141.

[20] M.A. Ahmed, N.M. Abdelbar, A.A. Mohamed, Molecular imprinted chitosan-TiO_2 nanocomposite for the selective removal of rose Bengal from wastewater, Int. J. Biol. Macromol., 107 (2018) 1046–1053.

[21] M.H. Rasoulifard, M.S.S. Dorraji, V. Mozafari, Visible light photo catalytic activity of chitosan/poly (vinyl alcohol)/TiO_2 nanocomposite for dye removal, Taguchi–based optimization, Environ. Prog. Sustain. Energy, 36 (2017) 66–72.

[22] B. Li, Y. Zhang, Y. Yang, W. Qiu, X. Wang, B. Liu, G. Sun, Synthesis, characterization, and antibacterial activity of chitosan/TiO_2 nanocomposite against Xanthomonas oryzae pv. oryzae, Carbohydr. Polym., 152 (2016) 825–831.

[23] Y. Kamari, M. Ghiaci, Preparation and characterization of ibuprofen/modified chitosan/TiO_2 hybrid composite as a controlled drug-delivery system, Micropor. Mesopor. Mater., 234 (2016) 361–369.

[24] X. Wu, X. Zhong, Y. Chai, R. Yuan, Electrochemiluminescence acetylcholine biosensor based on biofunctional AMs-AChE-ChO biocomposite and electro deposited graphene-Au-chitosan nanocomposite, Electrochim. Acta, 147 (2014) 735–742.

[25] A.H. Jawad, M.A. Nawi, Oxidation of cross linked chitosan-epichlorohydrine film and its application with TiO_2 for phenol removal, Carbohydr. Polym., 90 (2012) 87–94.

[26] S. Karimifard, M.R.A. Moghaddam, Application of response surface methodology in physicochemical removal of dyes from wastewater, A critical review, Sci. Total Environ., 640 (2018) 772–797.

[27] A.T. Mohammad, A.S. Abdulhameed, A.H. Jawad, Box-Behnken design to optimize the synthesis of new cross linked chitosan-glyoxal/TiO_2 nanocomposite: Methyl orange adsorption and mechanism studies, Int. J. Biol. Macromol., 129 (2019) 98–109.

[28] M.K. Uddin, U. Baig, Synthesis of Co_3O_4 nanoparticles and their performance towards methyl orange dye removal: Characterisation, adsorption and response surface methodology, J. Clean. Prod., 211 (2019) 1141–1153.

[29] A.H. Jawad, A.F.M. Alkarkhi, N.S.A. Mubarak, Photo catalytic decolorization of methylene blue by an immobilized TiO_2 film under visible light irradiation: optimization using response surface methodology (RSM), Desal. Water Treat., 56(1) (2015) 161–172.

[30] J.E. Silveira, E.M.T. Claro, W.S. Paz, A.S. Oliveira, J.A. Zazo, J.A. Casas, Optimization of Disperse Blue 3 mineralization by UV-LED/$FeTiO_3$ activated persulfate using response surface methodology, J. Taiwan Inst. Chem. Eng., 85 (2018) 66–73.

[31] E. Natarajan, G.P. Ponnaiah, Optimization of process parameters for the decolorization of Reactive Blue 235 dye by barium alginate immobilized iron nanoparticles synthesized from aluminum industry waste, Environ. Nanotechnol. Monit. Manage., 7 (2017) 73–88.

[32] A.Z. Moghaddam, E. Ghiamati, A. Pourashuri, A. Allahresani, Modified nickel ferrite nanocomposite/functionalized chitosan as a novel adsorbent for the removal of acidic dyes, Int. J. Biol. Macromol., 120 (2018) 1714–1725.

[33] P.A. Nishad, A. Bhaskarapillai, S. Velmurugan, Enhancing the antimony sorption properties of nano titania-chitosan beads using epichlorohydrin as the cross linker, J. Hazard. Mater., 334 (2017) 160–167.

[34] J. Maity, S.K. Ray, Chitosan based nano composite adsorbent—Synthesis, characterization and application for adsorption of binary mixtures of Pb (II) and Cd (II) from water, Carbohydr. Polym., 182 (2018) 159–171.

[35] R. Huang, Q. Liu, J. Huo, B. Yang, Adsorption of methyl orange onto protonated cross-linked chitosan, Arab. J. Chem., 10 (2017) 24–32.

[36] Z.A. Al-Othman, R. Ali, M. Naushad, Hexavalent chromium removal from aqueous medium by activated carbon prepared from peanut shell: adsorption kinetics, equilibrium and thermodynamic studies, Chem. Eng. J., 184 (2012) 238–247.

[37] S. Lagergren, Zur theorie der sogenannten adsorption geloster stoffe. Kungliga svenska vetenskapsakademiens, Handlingar, 24 (1898) 1–39.

[38] Y.S. Ho, G. McKay, Sorption of dye from aqueous solution by peat, Chem. Eng. J., 70 (1998) 115–124.

[39] I. Langmuir, The adsorption of gases on plane surfaces of glass, mica and platinum, J. Am. Chem. Soc., 40 (1918) 1361–1403.

[40] H.M.F. Freundlich, Over the adsorption in solution, J. Phys. Chem., 57 (1906) 385–471.

[41] M.I. Temkin, Kinetics of ammonia synthesis on promoted iron catalysts, Acta Physiochim. URSS, 12 (1940) 327–356.

[42] S. Prakash, M. Kumar, B.P. Tripathi, V.K. Shahi, Sol–gel derived poly (vinyl alcohol)-3-(2-aminoethylamino) propyl trimethoxysilane: cross-linked organic–inorganic hybrid beads for the removal of Pb (II) from aqueous solution, Chem. Eng. J., 162 (2010) 28–36.

[43] J.W. Lee, S.P. Choi, R. Thiruvenkatachari, W.G. Shim, H. Moon, Submerged micro filtration membrane coupled with alum coagulation/powdered activated carbon adsorption for complete decolorization of reactive dyes, Water Res., 40 (2006) 435–444.

[44] A.H. Jawad, M.A. Islam, B.H. Hameed, Cross-linked chitosan thin film coated onto glass plate as an effective adsorbent for adsorption of reactive orange 16, Int. J. Biol. Macromol., 95 (2017) 743–749.

[45] T.Y. Kim, J.W. Lee, S.Y. Cho, Application of residual brewery yeast for adsorption removal of reactive orange 16 from aqueous solution, Adv. Powder Technol., 26 (2015) 267–274.

[46] V. Anaki, K. Vijayaraghavan, A.K. Ramasamy, K.J. Lee, B.T. Oh, S. Kamala-Kannan, Competitive adsorption of Reactive Orange 16 and Reactive Brilliant Blue R on polyaniline/bacterial extracellular polysaccharides composite—A novel eco-friendly polymer, J. Hazard. Mater., 241 (2012) 110–117.

[47] A.R. Nesic, A. Onjia, S.J. Velickovic, D.G. Antonovic, Preparation and characterisation of novel biodegradable material based on chitosan and poly (Itaconic Acid) as adsorbent for removal of reactive orange 16 dye from wastewater, Sustain. Develop. Know. Soc. Smar. Fut. Manufact. Technol. Springer, Cham., (2015) 243–251.

[48] T. Calvete, E.C. Lima, N.F. Cardoso, J.C. Vaghetti, S.L. Dias, F.A. Pavan, Application of carbon adsorbents prepared from Brazilian-pine fruit shell for the removal of reactive orange 16 from aqueous solution: kinetic, equilibrium, and thermodynamic studies, J. Environ. Manage., 91 (2010) 1695–1706.

[49] F. Marrakchi, W.A. Khanday, M. Asif, B.H. Hameed, Cross-linked chitosan/sepiolite composite for the adsorption of methylene blue and reactive orange 16, Int. J. Biol. Macromol., 93 (2016) 1231–1239.

[50] M. Auta, B.H. Hameed, Optimized and functionalized paper sludge activated with potassium fluoride for single and binary adsorption of reactive dyes, J. Ind. Eng. Chem., 20 (2014) 830–840.

[51] P. Ramachandran, R. Vairamuthu, S. Ponnusamy, Adsorption isotherms, kinetics, thermodynamics and desorption studies of reactive orange 16 on activated carbon derived from Ananas comosus(L.) carbon, J. Eng. Appl. Sci., 6 (2011) 15–26.

[52] S.W. Won, S.B. Choi, Y.S. Yun, Performance and mechanism in binding of reactive orange 16 to various types of sludge, Biochem. Eng. J., 28 (2006) 208–214.

[53] F. Marrakchi, M.J. Ahmed, W.A. Khanday, M. Asif, B.H. Hameed, Mesoporous carbonaceous material from fish scales as low-cost adsorbent for reactive orange 16 adsorption, J. Taiwan Inst. Chem. Eng., 71 (2017) 47–54.

[54] N.F. Cardoso, E.C. Lima, T. Calvete, I.S. Pinto, C.V. Amavisca, T.H. Fernandes, W.S. Alencar, Application of aqai stalks as biosorbents for the removal of the dyes Reactive Black 5 and Reactive Orange 16 from aqueous solution, J. Chem. Eng. Data., 56 (2011) 1857–1868.

[55] S.T. Ong, C.K. Lee, Z. Zainal, Removal of basic and reactive dyes using ethylenediamine modified rice hull, Bioresour. Technol., 98 (2007) 2792–2799.

[56] A.M.D. Jesus, L.P.C. Romão, B.R. Araújo, A.S. Costa, J.J. Marques, Use of humin as an alternative material for adsorption/desorption of reactive dyes, Desalination, 274 (2011) 13–21.

[57] D.A. Fungaro, S.I. Borrely, T.E. Carvalho, Surfactant modified zeolite from cyclone ash as adsorbent for removal of Reactive Orange 16 from aqueous solution, Am. J. Environ. Prot., 1 (2013) 1–9.

[58] H.L. Parker, A.J. Hunt, V.L. Budarin, P.S. Shuttleworth, K.L. Miller, J.H. Clark, The importance of being porous: polysaccharide-derived mesoporous materials for use in dye adsorption, RSC Adv., 2 (2012) 8992–8997.

[59] S.K. Singh, A. Das, The n → π* interaction: a rapidly emerging non-covalent interaction, Phys. Chem. Chem. Phys., 17 (2015) 9596–9612.

[60] M. Mirabedini, M.Z. Kassaee, S. Poorsadeghi, Novel magnetic chitosan hydro gel film, cross-linked with glyoxal as an efficient adsorbent for removal of toxic Cr (VI) from water, Arab. J. Sci. Eng., 42 (2017) 115–124.

[61] M. Monier, D.M. Ayad, D.A. Abdel-Latif, Adsorption of Cu (II), Cd (II) and Ni (II) ions by cross-linked magnetic chitosan-2-aminopyridine glyoxal Schiff's base, Colloids Surf. B Biointerfaces, 94 (2012) 250–258.

[62] X. Chang, D. Chen, X. Jiao, Chitosan-based aerogels with high adsorption performance, J. Phys. Chem. B., 112 (2008) 7721–7725.